Virginia Commonwealth University
VCU Scholars Compass

Electrical and Computer Engineering Publications

Dept. of Electrical and Computer Engineering

2012

Anisotropy of free-carrier absorption and diffusivity in m-plane GaN

P. Ščajev
Institute of Applied Research

K. Jarašiūnas
Institute of Applied Physics, Virginia Commonwealth University

U. Ozgur
Virginia Commonwealth University, uozgur@vcu.edu

See next page for additional authors

Authors
P. Ščajev, K. Jarašiūnas, U. Ozgur, Hadis Morkoç, J. Leach, and T. Paskova

Anisotropy of free-carrier absorption and diffusivity in m-plane GaN

P. Ščajev,[1,a)] K. Jarašiūnas,[1,2] Ü. Özgür,[2] H. Morkoç,[2] J. Leach,[3] and T. Paskova[3]

[1]*Institute of Applied Research, Vilnius University, Saulėtekio Ave. 9 - III, Vilnius 10222, Lithuania*
[2]*Department of Electrical and Computer Engineering, Virginia Commonwealth University, Richmond, Virginia 23284, USA*
[3]*Kyma Technologies, Inc., 8829 Midway West Road, Raleigh, North Carolina 27617, USA*

Polarization-dependent free-carrier absorption (FCA) in bulk m-plane GaN at 1053 nm revealed approximately 6 times stronger hole-related absorption for E⊥c than for E||c probe polarization both at low and high carrier injection levels. In contrast, FCA at 527 nm was found isotropic at low injection levels due to electron resonant transitions between the upper and lower conduction bands, whereas the anisotropic impact of holes was present only at high injection levels by temporarily blocking electron transitions. Carrier transport was also found to be anisotropic under two-photon excitation, with a ratio of 1.17 for diffusivity perpendicular and parallel to the c-axis. © *2012 American Institute of Physics*. [doi:10.1063/1.3674306]

Development of nonpolar and semipolar GaN-based devices has been gaining interest as the polarization induced fields in the commonly employed polar c-plane orientation hamper the efficiency of light emitters and brings about constraints on the widths of quantum wells used in active regions. For device designs utilizing nonpolar and semipolar orientations, it is imperative that anisotropy of optical and electrical properties of wurtzite type nitrides is considered. However, the anisotropy of carrier transport or polarization-dependent absorption have not been investigated in sufficient detail, as the earlier studies utilized relatively thin c-plane GaN platelets which restricted the propagation of a probing optical beam along the symmetry axis (k||c, E⊥c). Heretofore, only the polarization-state of emission in thin nonpolar m-plane GaN films has been investigated, confirming the polarization selection rules and revealing an anisotropic strain.[1,2]

Bulk nonpolar crystals allow coupling of an optical probe conveniently along or perpendicular to the c-axis and thus investigation of the anisotropic features. Indeed, a strong anisotropy of free-carrier absorption (FCA) has been observed in heavily doped hexagonal n-SiC polytypes due to anisotropy of electron effective mass.[3,4] In nitride semiconductors, the valence band splitting and spin-orbit interaction lead to more favorable conditions for the hole-related FCA,[5] and the indirect absorption processes have been numerically analyzed for GaN/InGaN heterostructures in the 400-670 nm spectral range.[6] The latter calculations predicted up to two times higher intraband absorption cross-section by holes for light polarized perpendicular to c-axis ($\sigma_{h\perp}$) than that for the parallel polarization ($\sigma_{h||}$) and rather weak isotropic absorption by free electrons. The experimental value of FCA for undoped c-GaN was reported for a bipolar free-carrier plasma only for the E⊥c polarization, providing a cross-section of $\sigma_{eh} = (2.5 \pm 0.3) \times 10^{-17}$ cm^2 at 1053 nm.[7]

Here, we report on an experimental study of free-carrier absorption and carrier transport in a nonpolar m-plane bulk GaN substrate using optical probes at $\lambda_p = 1053$ and 527 nm.

Taking advantage of the in-plane c-axis, we were able to investigate the anisotropy by directing the linearly polarized probe beam normal to the surface and rotating its polarization for full 360°. Measurements of polarization-dependent FCA revealed nearly 6-times stronger hole-related absorption at 1053 nm for E⊥c as compared to that for E||c. Isotropic and rather strong FCA was measured at 527 nm which we attributed to FCA in the conduction bands. The anisotropy of ambipolar and hole diffusivity was found to be much less pronounced.

The measurements were carried out on a $d = 450\,\mu$m-thick m-plane freestanding GaN wafer, sliced from a 7-mm thick freestanding Hydride Vapor Phase Epitaxy (HVPE) grown GaN boule (with an electron density of 9.5×10^{15} cm^{-3}, threading dislocation density varying from $\sim 1 \times 10^6$ cm^{-2} at the edge side to $\sim 4 \times 10^5$ cm^{-2} at the front side of the boule). For carrier injection to the entire bulk of the layer, we used two-photon (2P) excitation by 15 ps pulses at 527 nm from a neodymium-doped yttrium lithium fluoride laser. Single-photon (1P) carrier injection at 351 nm was used to reach higher injected carrier densities, in a photopumped slice of thickness δ. Monitoring the probe beam differential transmission, $\ln(T_0/T) = \Delta\alpha\delta$, we measured the FCA coefficient, $\Delta\alpha$, at $\lambda_p = 1053$ nm and 527 nm probe wavelengths and determined the FCA cross-sections $\sigma_{eh} = \ln(T_0/T)/\int \Delta N(z)dz$, where the injected carrier density $\Delta N(z)$ is integrated over the sample thickness.[5] By varying the orientation of the linearly polarized probe beam with respect to the c-axis, the anisotropy of σ_{eh} was measured. Carrier diffusivity was investigated by the light-induced transient grating technique[8] under two-photon injection conditions, providing $\Delta N = 10^{16} - 5 \times 10^{17}$ cm^{-3}. Two orthogonal orientations of the grating vector K with respect to the c-axis were used to determine the diffusion coefficient D along the two orthogonal directions ($K\perp$c and $K||$c) from the diffusion-governed grating decay time.

In Fig. 1(a), we present the dependence of FCA on excitation energy density for 1053 nm probe. The FCA signal increased almost linearly with carrier injection at 351 nm, thus a constant σ_{eh} value can be assumed in the range up to

---

a)Author to whom correspondence should be addressed. Electronic mail: patrik.scajev@ff.vu.lt. Telephone: +370 5 2366036. Fax: +370 5 2366037.
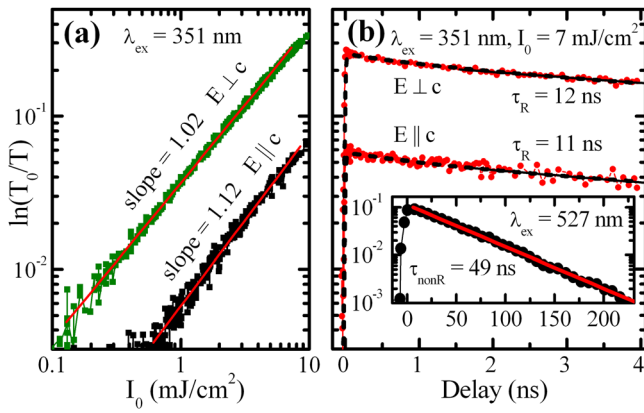
FIG. 1. (Color online) (a) Polarization-dependent FCA for a 1053 nm probe beam: dependence on excitation energy density and (b) FCA decay kinetics at high injected carrier density (5×10^{19} cm^{-3}). The dashed lines are numerical fits and the inset in (b) shows FCA decay at low excess carrier density ($\sim 10^{17}$ cm^{-3}).

7 mJ/cm^2 ($\sim 5 \times 10^{19}$ cm^{-3}). The linear relationship allowed us to determine σ_{eh} values. A varying FCA signal strength for different probe beam polarizations implies that σ_{eh} is strongly anisotropic [Fig. 2(a)]. The FCA cross-section as a function of the polarization angle ϕ was fitted using $\sigma_{eh}(\phi) = \sigma_{eh\perp} - (\sigma_{eh\perp} - \sigma_{eh\parallel}) \cos^2(\phi)$. For the 1053 nm probe, we obtained $\sigma_{eh\perp} = 2.2 \times 10^{-17}$ cm^2, $\sigma_{eh\parallel} = 3.4 \times 10^{-18}$ cm^2, and an anisotropy ratio $S = \sigma_\perp/\sigma_\parallel = 6.5$. The same values of σ_{eh} and S were obtained under two photon excitation, i.e., in the carrier density range from 10^{15} to 5×10^{17} cm^{-3} [see
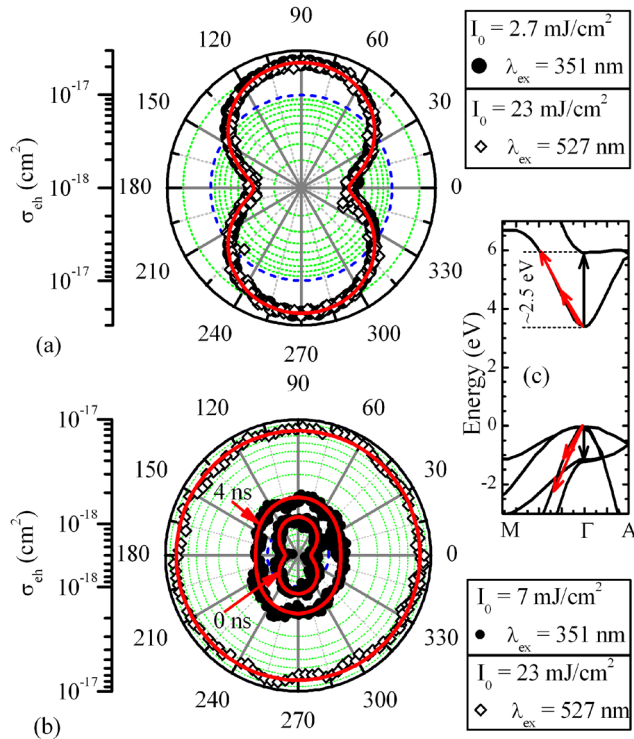

FIG. 2. (Color online) (a) Polarization dependence of FCA cross-section σ_{eh} for 1053 nm probe wavelength at high (351 nm) and low injection (527 nm) conditions. (b) σ_{eh} for 527 nm probe at low ($\Delta N \sim 5 \times 10^{17}$ cm^{-3}, external circle) and high injection [two internal circles for σ_{eh} at zero delay time (for $\Delta N \sim 5 \times 10^{19}$ cm^{-3}) and at 4 ns delay time (for $\Delta N \sim 2.6 \times 10^{19}$ cm^{-3})]. (c) GaN energy band diagram with direct (vertical arrows) and indirect phonon-assisted intraband transitions (diagonal arrows) depicted (after Ref. 6).

Fig. 2(a)]. The injection-independent FCA at the given probe wavelength can be attributed to the polar optical phonon assisted FCA in valence bands,[6] thus $\sigma_{eh} \approx \sigma_h$ at 1053 nm.

Polarization-dependent FCA measurements with the 527 nm probe were performed at low and high carrier injection conditions (i.e., by using excitation wavelengths of 527 nm or 351 nm, respectively). At low excess carrier densities, the measurements yielded smaller σ_{eh} values compared to those for the 1053 nm probe and no dependence on polarization: $\sigma_{eh\perp} = \sigma_{eh\parallel} = 8 \times 10^{-18}$ cm^2 [Fig. 2(b)]. This is a clear signature that holes that are responsible for FCA anisotropy at 1053 nm do not contribute noticeably to FCA in the visible spectral range, or at least at 527 nm. Therefore, the electron-related transitions within the conduction band must be invoked, contrary to the predictions.[6] The measured FCA cross-section that is more than an order of magnitude larger than the predicted one $\sigma_e = 4.6 \times 10^{-19}$ cm^2 is ascribed to the isotropic conduction bands.[9] The contribution of direct inter-valence-band hole transitions cannot be observed at 527 nm due to absence of appropriate valence bands [see Fig. 2(c)].[6]

At high injection levels, the measured FCA cross sections for $\lambda_p = 527$ nm revealed anisotropic features and much smaller σ_{eh} values with respect to those measured under low injection [Fig. 2(b)]. We note that the high injection σ_{eh} values measured at zero delay [$\sigma_{eh\perp} = 1.2 \times 10^{-18}$ cm^2, $\sigma_{eh\parallel} = 6.7 \times 10^{-19}$ cm^2, and $S = \sigma_\perp/\sigma_\parallel = 1.8$, see Fig. 2(b)] are close to the theoretical values for holes ($\sigma_{h\perp} = 1.5 \times 10^{-18}$ cm^2, $\sigma_{h\parallel} = 6.2 \times 10^{-19}$ cm^2, $S = \sigma_\perp/\sigma_\parallel = 2.4$),[6] thus indicating that interband transitions in the conduction band are fully suppressed at high excess carrier densities. Moreover, at longer probe delays, σ_{eh} values slightly increased and became more isotropic [Fig. 2(b)]: at 4 ns delay, $\sigma_{eh\perp} = 1.8 \times 10^{-18}$ cm^2, $\sigma_{eh\parallel} = 1.3 \times 10^{-18}$ cm^2, and $S = \sigma_\perp/\sigma_\parallel = 1.4$.

To understand these observations, we analyzed the rate of nonequilibrium processes and the influence of high excess carrier density on the intraband transitions within the conduction bands. Single-photon excitation at 351 nm provides a carrier density of up to $\Delta N \sim 10^{20}$ cm^{-3} within a very thin photoexcited layer, $\delta = 1/\alpha = 0.1$ μm, but ongoing rather fast diffusion processes as well as the plausible absorption bleaching for 351 nm wavelength may expand the excited layer thickness δ up to a few micrometers.[8] The injection-density (ΔN) dependent room-temperature bandgap, according to Ref. 10 is given by $E_{g,opt}(\Delta N)$ [eV] $= 3.452 - 4.27 \times 10^{-8} \times \Delta N^{1/3} + 0.082 \times (\Delta N/10^{19})^{2/3}$, where the second and the third terms on the right hand side represent the band gap renormalization (BGR) and band filling, respectively. Consequently, for the employed excitation wavelength of 351 nm ($h\nu_3 = 3.53$ eV), the injected average carrier density for $I_0 = 7$ mJ/cm^2 fluence is limited to $N^* = 4.8 \times 10^{19}$ cm^{-3} [assuming that $E_{g,opt}(N^*) = h\nu_3$], and, therefore, carriers are distributed over $\delta = 2.6$ μm depth, since $N^* \times \delta = I_0/h\nu_3$. In order to obtain the carrier density at 4 ns delay time [Fig. 1(b)], we fitted the FCA decay rate using the relationship $1/\tau_R = 1/\tau_{nonR} + B(\Delta N) \times \Delta N$ and the measured nonradiative carrier lifetime of $\tau_{nonR} = 49$ ns at low injection (see inset in [Fig. 1(b)]). The modeling of vertical carrier diffusion with varying diffusivity $D(\Delta N)$ and bimolecular recombination coefficient $B(\Delta N)$ values for the degenerate carrier plasma[11,12]

provided a density of 2.6×10^{19} cm^{-3} and an instantaneous lifetime of 11 ns at 4 ns delay. As the hole effective mass is some 10 times higher than that for electrons,[10] band filling and BGR impact the conduction band more by lifting it up by 233 meV and shifting down by 155 meV, respectively, [obtained from $E_{g,opt}(\Delta N)$ at $\Delta N = N^*$]. Assuming that higher energy electrons mostly contribute to interband transitions leads to detuning of the resonance transition energy between lower and upper conduction bands at ~ 2.5 eV (Ref. 6) and to vanishing electron-related contribution to σ_{eh} (see Fig. 2(c)). At longer probe delays, the impact of many-body effects decreases with decreasing carrier density causing the FCA cross-section to increase. Eventually, at the low injection limit ($\sim 10^{17}$ cm^{-3}), the measured $\sigma_{eh} = 8 \times 10^{-18}$ cm^2 value involves contributions from the isotropic electron cross-section, $\sigma_e = 7 \times 10^{-18}$ cm^2, and the much smaller anisotropic hole cross-section, $\sigma_h \approx (1.2\text{-}0.7) \times 10^{-18}$ cm^2, measured at zero delay [see Fig. 2(b)].

The fitting of σ_h in the 527-1064 nm range uncovered a tendency of its fast increase in accordance with the relationship $\sigma_h \propto \lambda^{-p}$, accounting both the anisotropy in effective masses and relaxation times.[6] Here, scattering by polar optical phonons would lead to $p = 2.5$ (Ref. 13) whereas our fitting provided p values of 4.0 and 2.5 for E$\perp$c and E$\parallel$c polarizations, respectively. The discrepancy with the theory for E$\perp$c polarization can be explained by band nonparabolicities and/or hole intervalence band transitions for 1053 nm.[6] Injection independent σ_h at 1053 nm is verified by a linear dependence of FCA vs. injection [as predicted theoretically[13] and confirmed by our data, Fig. 1(a)] and vs. temperature (as reported for E$\perp$c (Ref. 7)).

For measurements of the diffusivity, D, the carriers were injected by two-photon interband transitions at 527 nm providing equal density of electrons and holes. The sample was rotated by 90° to obtain the orthogonal or parallel orientations of the grating vector $K = 2\pi/\Lambda$ (which is in the plane of grating recording beams) with respect to the c-axis. The refractive index spatial modulation $\Delta n(x)$ by the injected carrier density $\Delta N(x) = N_{02P}(1 + \cos(Kx))^2$, where x is the in-plane spatial coordinate, creates a transient phase grating [$\Delta n(x) \propto \Delta N(x)$], on which the probe beam at 1053 nm diffracts and its efficiency decays with $\eta(t) \propto \Delta N^2 \exp(-2t/\tau_G)$.[14] The measured exponential grating decay time τ_G is used to obtain the diffusive decay time $\tau_D = 1/K^2 D$ through the relationship $1/\tau_G = 1/\tau_R + 1/\tau_D$ for the given diffusion coefficient D, grating period $\Lambda = 1.74$ μm and a very long nonradiative carrier lifetime $\tau_R \approx \tau_{nonR} = 49$ ns. Two-photon band-to-band excitation created holes and electrons with equal densities $\Delta N = \Delta N_n = \Delta N_h$, and the injected average carrier density $N_{av} = 1.5 \times N_{02P}$ was calculated according to Ref. 14. The electrons and holes diffused together with the ambipolar diffusion coefficient given as:[15] $D(\Delta N) = (n_0 + \Delta N_n + \Delta N_h)D_n D_h / [(n_0 + \Delta N_n)D_n + \Delta N_h D_h]$, where n_0 is the doped electron density and D_h and D_n are the hole and electron diffusivities, respectively. Assuming that $D_h \ll D_n$ for GaN due to the large hole effective mass, we determined the D_h value at low injections ($\Delta N \ll n_0$) and the ambipolar diffusivity $D_a \sim 2D_h$ at $\Delta N \gg n_0$. A fitting of experimental diffusivity data (Fig. 3) as a function of N_{av} provided an average doping density of $n_0 = 2 \times 10^{16}$ cm^{-3} as well as hole diffusion coefficients of
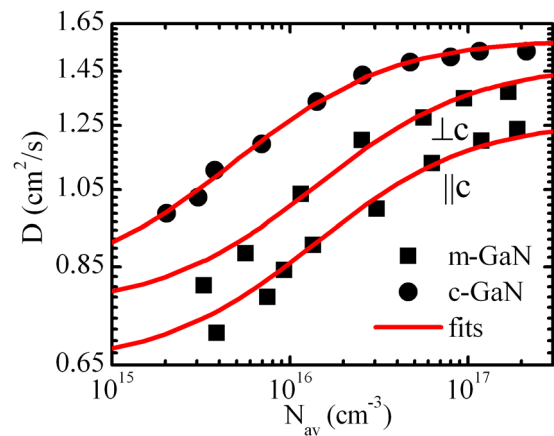

FIG. 3. (Color online) Anisotropy of diffusivity in bulk m-GaN. For comparison, the D values for free-standing c-GaN (with dislocation density 5×10^5 cm^{-2}) revealed a slightly higher $D_{h\perp} = 0.81$ cm/s value due to lower doping ($n_0 = 8 \times 10^{15}$ cm^{-3}).

$D_{h\perp} = 0.76$ cm^2/s and $D_{h\parallel} = 0.65$ cm^2/s. For modeling the diffusivity at low injections, D_n values of 36 and 26 cm^2/s were used for c-plane and m-plane samples, respectively, based on the reported electron mobilities[16] and their relationship to diffusivity, $D_n = kT\mu_e/e$.[15] The experimental data provided a 17% anisotropy of the room-temperature hole mobility in m-plane GaN for two orthogonal in-plane orientations. The rather small anisotropy of mobility can be attributed to the opposite anisotropy of the light-hole and split-off valence bands.[9] In the m-plane GaN sample investigated, the acoustic phonon scattering is dominant at room temperature, as the ionized impurity scattering reduces the mobility in m-GaN with respect to c-GaN only by 7% based on the doping levels. Thus, according to Ref. 17, a ratio of $D_\perp/D_\parallel = 1.35$ was calculated, using the GaN valence band parameters.[9] The calculated diffusion anisotropy is in satisfactory agreement with the experimentally obtained value of $D_\perp/D_\parallel = 1.17$.

In conclusion, we investigated the FCA anisotropy and diffusivity in bulk m-plane GaN under low and high carrier injection conditions. A strong hole-related FCA anisotropy was observed at 1053 nm probe wavelength with the cross-section ratio of $\sigma_\perp/\sigma_\parallel = 6.5$. FCA at 527 nm probe wavelength was isotropic and related to electron-transitions between the lower and upper conduction bands. Strong blocking of electron transitions at high injections due to band filling and renormalization revealed the anisotropic features of hole-related FCA at 527 nm. Small anisotropy of hole and ambipolar diffusivity was attributed to the opposite anisotropy of the light-hole and split-off valence bands.

[1]P. Paskov, T. Paskova, P. O. Holtz, and B. Monemar, Phys. Rev. B **70**, 035210 (2004).
[2]C. Rivera, P. Misra, J. L. Pau, E. Muñoz, O. Brandt, H. T. Grahn, and K. H. Ploog, J. Appl. Phys. **101**, 053527 (2007).
[3]B. Ellis and T. S. Moss, Solid State Commun. **3**, 109 (1965).
[4]V. Grivickas, A. Galeckas, P. Grivickas, and J. Linnros, Mater. Sci. Forum **338–342**, 555 (2000).
[5]P. Ščajev, V. Gudelis, K. Jarašiūnas, and P. B. Klein, J. Appl. Phys. **108**, 023705 (2010).

[6]E. Kioupakis, P. Rinke, A. Schleife, F. Bechstedt, and C. G. Van de Walle, Phys. Rev. B **81**, 241201(R) (2010).

[7]P. Ščajev, A. Usikov, V. Soukhoveev, R. Aleksiejūnas, and K. Jarašiūnas, Appl. Phys. Lett. **98**, 202105 (2011).

[8]T. Malinauskas, K. Jarašiūnas, S. Miasojedovas, S. Juršėnas, B. Beaumont, and P. Gibart, Appl. Phys. Lett. **88**, 202109 (2006).

[9]Y. C. Yeo, T. C. Chong, and M. F. Li, J. Appl. Phys. **83**, 1429 (1998).

[10]M. Yoshikawa, M. Kunzer, J. Wagner, H. Obloh, P. Schlotter, R. Schmidt, N. Herres, and U. Kaufmann, J. Appl. Phys. **86**, 4400 (1999).

[11]T. Malinauskas, K. Jarašiūnas, M. Heuken, F. Scholz, and P. Brukner, Phys. Status Solidi C **6**, S743 (2009).

[12]For modeling, a lower $B = 0.3 \times 10^{-11}$ cm^3/s was used with respect to a low-injection one, $B = (2\text{-}5) \times 10^{-11}$ cm^3/s.

[13]B. K. Ridley, *Quantum Processes in Semiconductors* (Clarendon, Oxford, 1999).

[14]P. Ščajev, V. Gudelis, E. Ivakin, and K. Jarašiūnas, Phys. Status Solidi A **208**, 2067 (2011).

[15]J. F. Schetzina and J. P. McKelvey, Phys. Rev. B **2**, 1869 (1970).

[16]D. Huang, F. Yun, M. A. Reshchikov, D. Wang, H. Morkoç, D. L. Rode, L. A. Farina, ç. Kurdak, K. T. Tsen, S. S. Park *et al.*, Solid State Electron. **45**, 711 (2001).

[17]T. Kinoshita, K. M. Itoh, M. Schadt, and G. Pensl, J. Appl. Phys. **85**, 8193 (1999).